Design of a New Optical Material with Broad Spectrum Linear and Two-Photon Absorption and Solvatochromism

ARTICLE · NOVEMBER 2013

DOI: 10.1021/jp406500t

8 AUTHORS, INCLUDING:

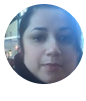

Iffat Nayyar

Pacific Northwest National Laboratory

16 PUBLICATIONS **138** CITATIONS

SEE PROFILE

Adam W Woodward

University of Central Florida

11 PUBLICATIONS **41** CITATIONS

SEE PROFILE

Kevin D Belfield

University of Central Florida

225 PUBLICATIONS **4,279** CITATIONS

SEE PROFILE

Artem E. Masunov

University of Central Florida

147 PUBLICATIONS **2,538** CITATIONS

SEE PROFILE

THE JOURNAL OF PHYSICAL CHEMISTRY C

Article

pubs.acs.org/JPCC

Design of a New Optical Material with Broad Spectrum Linear and Two-Photon Absorption and Solvatochromism

William V. Moreshead,[†] Olga V. Przhonska,[‡] Mykhailo V. Bondar,[‡] Alexei D. Kachkovski,[§] Iffat H. Nayyar,[∥,⊥] Artëm E. Masunov,[†,∥,⊥,#] Adam W. Woodward,[†] and Kevin D. Belfield*[,†,▽]

[†]Department of Chemistry, University of Central Florida, P.O. Box 162366, Orlando, Florida, 32816, United States

[‡]Institute of Physics, National Academy of Sciences, Kiev, 03028, Ukraine

[§]Institute of Organic Chemistry, National Academy of Sciences, Kiev, 03094, Ukraine

[∥]NanoScience Technology Center, University of Central Florida, Orlando, Florida, 32826, United States

[⊥]Department of Physics, University of Central Florida, Orlando, Florida, 32816, United States

[#]Florida Solar Energy Center, University of Central Florida, Cocoa, Florida, 32922, United States

[▽]CREOL, The College of Optics and Photonics, University of Central Florida, Orlando, Florida, 32816, United States

Supporting Information

ABSTRACT: A fluorene-bridged squaraine dimer (SD-FLU-SD) was designed with the purpose of combining various chromophores in one molecule and enhancing its two-photon absorption properties using intra- and interchromophore transitions. Linear and nonlinear absorption properties of SD-FLU-SD were investigated with the goals of understanding the nature of one- and two-photon absorption spectra, determining the molecular optical parameters, and performing modeling of the photophysical processes. The optical behavior of this new SD-FLU-SD "hybrid" molecule was compared with its separate squaraine constituent moiety. Linear spectroscopic characterization includes absorption, fluorescence, excitation and emission anisotropy, and quantum yield measurements in solvents of different polarity and viscosity. Spectral positions of the absorption−fluorescence peaks and quantum yields of SD-FLU-SD and its separate squaraine moiety exhibited complex and nontrivial behavior as a function of solvent polarity. Comprehensive study of this unusual solvatochromism was conducted and interpreted using various models. Nonlinear spectroscopic studies included two-photon absorption measurements using the femtosecond Z-scan technique. The two-photon absorption spectrum of SD-FLU-SD was broad, covering the spectral range from 800 to 1400 nm with a maximum two-photon absorption cross section of 2 750 GM (1 GM = 1×10^{-50} cm^4 s/photon). Quantum chemical analysis, based on time-dependent density functional theory, agreed with the experimental data and revealed details on the energy-level structure and origin of the linear and nonlinear absorption behavior of this novel SD-FLU-SD compound. These investigations advance the understanding of the nature of electronic transitions and the structure−property relations in long conjugated molecules, which are important for the rational design of new organic optical materials.

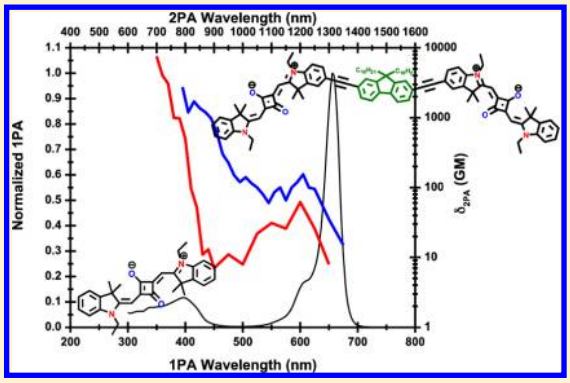

1. INTRODUCTION

Substantial efforts have been invested in the design, synthesis, and characterization of dyes with larger optical nonlinearities, with the ultimate goal of understanding structure−property relations in order to enable the rational design of the optical materials with linear and nonlinear optical properties optimized for specific applications. Organic compounds that have attracted significant attention include various fluorene (FLU) derivates as well as linear polymethines and related structures, such as squaraine dyes (SD). In both classes, fluorenes and polymethines, the linear and nonlinear optical (NLO) properties can be tailored via specific structural modifications.

Fluorene derivatives have been extensively studied because of their important role in a wide variety of NLO applications, including two-photon laser-scanning fluorescence microscopy and biological labeling,[1−4] 3D microfabrication and optical data storage,[5−7] two-photon photodynamic therapy,[8,9] stimulated emission depletion,[10,11] and upconverted lasing.[12,13] Many aspects of the optical and electronic properties of fluorenes are fairly well understood; for example, see refs 14 and 15 and references therein.

Received: July 1, 2013
Revised: October 7, 2013
Published: October 28, 2013

   dx.doi.org/10.1021/jp406500t | J. Phys. Chem. C 2013, 117, 23133−23147

Scheme 1. Synthesis of Bromo-Squaraine Derivative 3

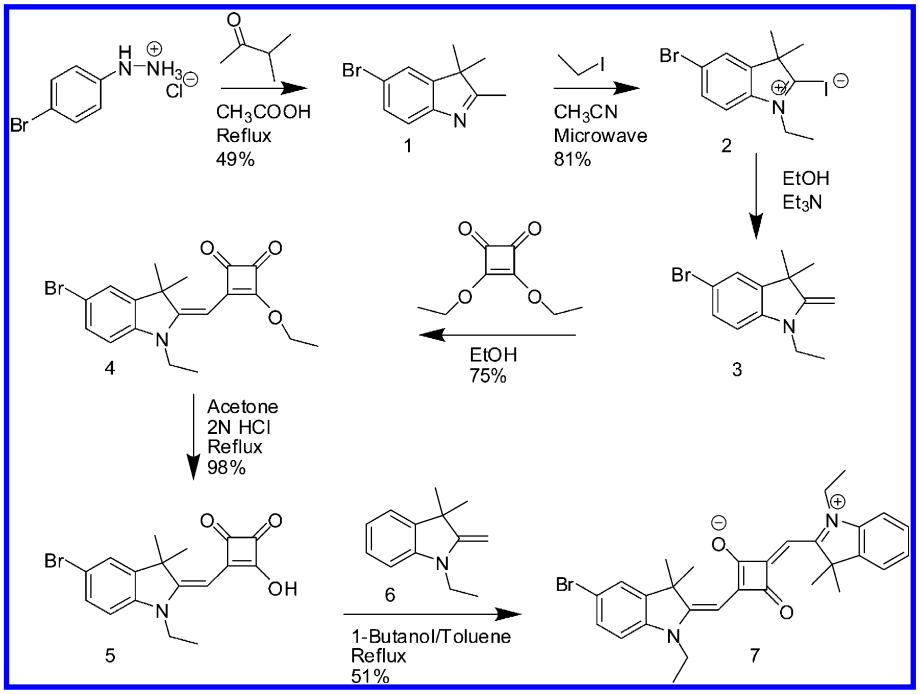

Linear polymethine-like structures, especially squaraines (which can be regarded as polymethines with a strong acceptor group C_4O_2 centered in the vinylene chain), have been shown to exhibit large two-photon absorption (2PA) cross sections (δ_{2PA}) of up to 35 000 GM[16] owing to very large ground-to-first excited state transition dipole moments, near-parallel orientation of their ground-to-first excited and between excited states transition dipole moments, and the sharply rising low-energy side of their linear absorption that allows significant intermediate-state resonance enhancement of the 2PA.[16−22] These molecules are also known for their significant singlet−singlet excited-state absorption (ESA) with peak cross sections of 10^{-16} to 10^{-15} cm^2, which are comparable to the peak ground-state absorption cross section.[23] The ratio between excited and ground-state cross sections can be as large as 200 at certain wavelengths, which is important for optical-limiting applications.[16,20−24]

The NLO properties, in particular two-photon absorption (2PA) spectra, for polymethines and related compounds have been intensively studied.[18−20,25,26] As discussed in ref 27, various strategies to increase 2PA in polymethine-like molecules include (1) lengthening of the effective π-conjugation length; (2) incorporation of a strong acceptor group into the conjugated bridge leading to a quadrupolar-type arrangement D-π-A-π-D (squaraine and tetraone structures); (3) exploiting the compounds with the sharply rising low-energy side of their linear absorption band decreasing the detuning energy and resulting in the strong intermediate-state resonance enhancement (squaraines); (4) proper choice of solvent polarity in unsymmetrical molecules; and (5) specific arrangement of the molecular energy levels allowing for an increase in the density of final states and reaching the final states at the smallest detuning energy (the so-called "double resonance" condition).

Photophysical and photochemical properties of the symmetrical and unsymmetrical squaraines have been reviewed (see refs 28−31). Symmetrical SDs are typically synthesized by the condensation of electron-rich compounds, usually arenes, with squaric acid. Unsymmetric SDs are most commonly synthesized in a two-step procedure via the hemisquaric acid ester intermediate (for example, Scheme 1).[32,33] The tremendous synthetic flexibility that these approaches afford has resulted in a great variety of squaraines explored for their potential applications as xerographic materials,[34] dye-sensitized solar cells,[35,36] histological probes,[37] ion sensors,[29,38] light-emitting field-effect transistors,[39] nonlinear optics,[40] sensitizers for photodynamic therapy,[41−44] and two-photon absorbing fluorescent probes for bioimaging.[45]

Both 1,2- and 1,3-disubstituted squaraines can be prepared depending upon the nature of the electron-rich arenes used, the synthetic route chosen, and the reaction conditions.[46,47] However, for this work we used only the 1,3-disubstituted squaraines because the 1,2-disubstituted squaraines do not demonstrate the same intense absorption, emission, and near-infrared (NIR) photophysical properties as described above for the corresponding 1,3-squaraines. It has been shown that 1,3-disubstituted squaraines have structures and properties similar to the polymethine dyes, while 1,2-squaraines more closely resemble the merocyanines.[47]

In this study, a SD-FLU-SD molecule consisting of two squaraine moieties bridged by a fluorene unit was designed, synthesized, and investigated with the goal of obtaining a detailed description of the linear and nonlinear optical properties. Fluorene and squaraines have been combined to produce dyes with red-shifted absorption especially for photovoltaic applications,[48−52] but to our knowledge this is the first report in which these groups are combined with the goal of enhancing and broadening two-photon absorption. The molecular linker is an alkyne (the triple bond) supporting the π-conjugation within the whole SD-FLU-SD molecule.[53,54] Our intent was to achieve a broadening of 2PA in the NIR spectral range by combining these two moieties into a single "hybrid" conjugated molecule.

dx.doi.org/10.1021/jp406500t | J. Phys. Chem. C 2013, 117, 23133−23147

Table 1. Measured Lifetimes, τ_{exp}; Radiative Lifetimes, τ_{rad}; Calculated Fluorescence Lifetimes, τ_{cal}; and Quantum Yields, Φ, for SD II and SD-FLU-SD I in Three Solvents

	SD-FLU-SD I			SD II		
solvent	TOL	THF	DCM[a]	TOL	THF	DCM
τ_{exp} (ns)	1.8 ± 0.3	1.4 ± 0.3	0.5 ± 0.1 (0.8) 1.6 ± 0.3 (0.2)	1.7 ± 0.3	1.2 ± 0.2	0.8 ± 0.2
τ_{rad} (ns)	1.7	2.3	2.2	3.2	2.8	2.7
τ_{cal} (ns)	0.8	0.8	0.6	1.6	0.8	0.6
Φ	0.53 ± 0.08	0.31 ± 0.05	0.25 ± 0.04	0.51 ± 0.08	0.30 ± 0.05	0.22 ± 0.03

[a]Amplitudes of the components for double-exponential decay of SD-FLU-SD I in DCM are shown in parentheses.

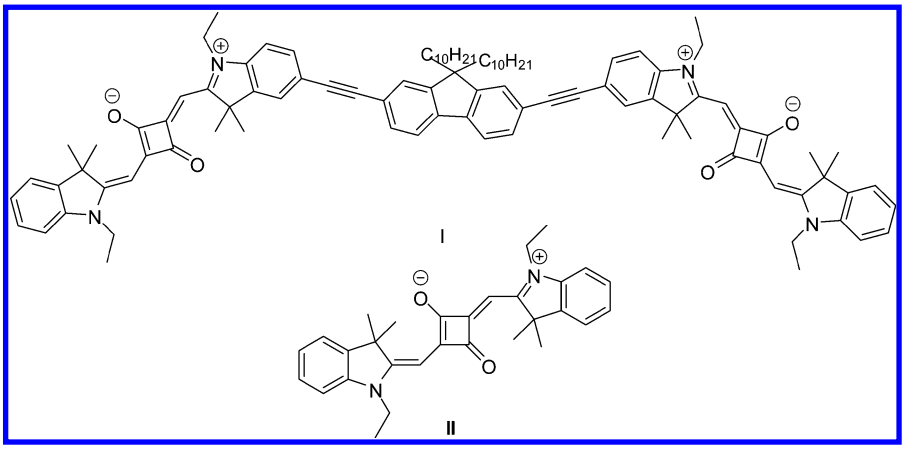

Figure 1. Structures of "hybrid" SD-FLU-SD compound I and the symmetrical squaraine II used as a model compound.

Herein, we present a detailed report on the photophysical properties of this compound. We describe the following: (1) synthesis of SD-FLU-SD compound; (2) linear absorption, fluorescence, and quantum yield of SD-FLU-SD and SD in several solvents; (3) thorough investigation of the role of solvent polarity on the quantum yields and positions of the absorption–fluorescence bands; (4) excitation and emission anisotropy of SD-FLU-SD and comparison with anisotropy of a symmetrical SD molecule; (5) 2PA measurements of both compounds using Z-scans with femtosecond pulsewidths; and (5) detailed quantum chemical calculations and modeling that provides insight into the nature of the linear and NLO properties. The combination of the experimental methods and theoretical analysis provides critical information regarding the energy-level structure, which agrees with the observed nonlinear absorption processes in the SD-FLU-SD compound.

2. EXPERIMENTAL SECTION

2.1. Synthetic Procedures. Full synthetic details and characterization data for all compounds synthesized in this work are provided in the Supporting Information.

2.2. Linear Characterization. The linear absorption spectra were obtained with an Agilent 8453 UV–visible spectrophotometer in 10 mm path length quartz cuvettes for dye concentrations of C = (10^{-5}–10^{-6}) M to avoid aggregation. The steady-state fluorescence and anisotropy spectra were measured in the photon-counting regime using a PTI QuantaMaster spectrofluorimeter in 10 mm spectrofluorometric quartz cuvettes with C ≈ 10^{-6} M. All fluorescence spectra were corrected for the spectral response of the PTI detection system. Linear spectroscopic measurements were conducted in solvents of different polarity and viscosity: toluene (TOL); tetrahydrofuran (THF); polytetrahydrofuran (pTHF); tiacetin (TAC); methanol (MeOH); dimethylsulfoxide (DMSO); acetonitrile (ACN); cyclohexane (CHX); 1-methylnaphthalene (1MN); *p*-cymene (CYM) dichloromethane (DCM); glycerol (GLY); and silicone oil, both polydimethylsiloxane (PDMS) and polymethylphenylsiloxane (PMPS), at room temperature. All solvents were of spectroscopic grade, when available, and used as received.

2.3. Lifetime Measurements. Fluorescence decay curves were measured in three solvents (TOL, THF, and DCM) using a PicoHarp 300 time-correlated single-photon counting system with a time resolution of ≈80 ps. The second harmonic of a Coherent Mira 900 fs laser system (220 fs pulse width, 76 MHz repetition rate) tuned to ≈800 nm was used for excitation. The linearly polarized laser beam at ≈400 nm was oriented at the magic angle to avoid possible effects of molecular rotation.[55,56] Experimental lifetimes, obtained from the fitting of the fluorescence decay curves, were compared with the lifetimes calculated according to $\tau_{cal} = \tau_R \Phi$, where Φ is the fluorescence quantum yield, and τ_R is the radiative lifetime calculated by the Birks–Dyson equation.[57] See Supporting Information for details of this calculation. Calculated and experimental lifetimes are listed in Table 1.

2.4. Two-Photon Absorption Measurements. The 2PA spectra of SD-FLU-SD I and SD II were obtained in DCM solution at room temperature by open-aperture Z-scan methodology, comprehensively described in reference 58. A simplified scheme of the femtosecond laser system (Coherent,

dx.doi.org/10.1021/jp406500t | J. Phys. Chem. C 2013, 117, 23133–23147

Scheme 2. Synthesis of SD-FLU-SD

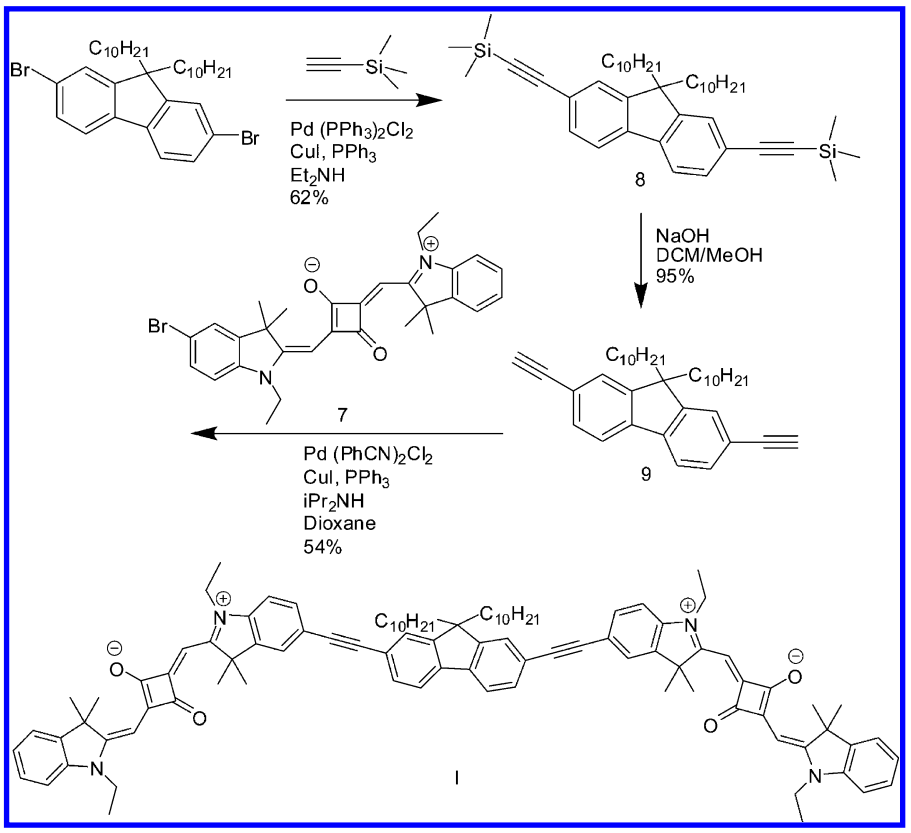

Scheme 3. Synthesis of Symmetrical Squaraine II

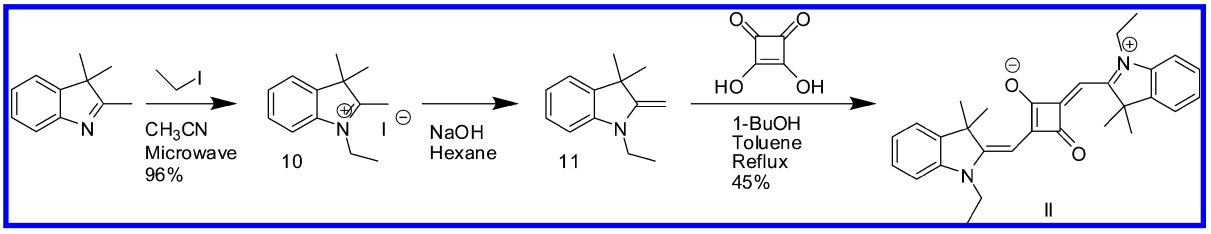

Inc.) is shown in Figure S1 of the Supporting Information. The output of mode-locked Ti:sapphire laser (Mira 900-F tuned to 800 nm, with average power of 1.2 W, pulse duration ≈180 fs, and repetition rate of 76 MHz), pumped by the second harmonic of Nd^{3+}:YAG laser (Verdi-10), was regeneratively amplified with 1 kHz repetition rate (Legend Elite), producing ≈100 fs pulses (fwhm) with pulse energy ≈3.5 mJ. This output at 800 nm was used for pumping an optical parametric amplifier (OPerA Solo) with exit pulse duration of ≈100 fs (fwhm), tuning range 240 nm to 20 μm, and pulse energies up to 200 μJ.

3. RESULTS AND DISCUSSION

3.1. Synthesis of SD-FLU-SD (I) and the Symmetrical Squaraine SD (II). The synthesis of the hybrid SD-FLU-SD compound **I** was accomplished by first synthesizing the unsymmetrical bromo-substituted squaraine **7** and then conjugating this to 2,7-diethynyl-9,9-didecylfluorene (**9**) via Sonogashira coupling. The well-known symmetrical squaraine **II** was synthesized and used as a model compound for comparison of photophysical properties with the hybrid SD-FLU-SD compound **I**. The structures of SD-FLU-SD **I** and SD model compound **II** are presented in Figure 1.

The synthesis of the unsymmetrical bromo-substituted squaraine **7** was accomplished in five steps, as shown in Scheme 1. First, the bromo-substituted indole **1** was synthesized via a Fisher condensation according to a literature method.[59] Alkylation of **1** was then accomplished in good yield using microwave radiation to give intermediate **2**. The corresponding methylene base **3** was then generated from this alkylated indole using base and reacted with diethylsquarate, yielding the hemisquaric acid ester **4**. The hemisquaric ester was hydrolyzed in refluxing acetone with 2N HCl to yield the corresponding acid **5**.[21] Reaction of intermediate **5** with the methylene base **6** was then accomplished with azeotropic removal of water to afford the unsymmetrical squaraine **7**.

Scheme 2 illustrates the synthetic scheme for SD-FLU-SD **I**. Sonogashira coupling was used to generate the trimethylsilyl-alkynylfluorene derivative **8**. Removal of the trimethylsilyl groups with sodium hydroxide in dichloromethane/methanol resulted in the diethynylfluorene intermediate **9**, which was then coupled with the bromo-substituted squaraine intermediate **7**, producing the desired SD-FLU-SD hybrid molecule **I**.

dx.doi.org/10.1021/jp406500t | J. Phys. Chem. C 2013, 117, 23133−23147

Synthesis of the symmetrical squaraine **II** was accomplished by reaction of the methylene base **11** with squaric acid with azeotropic removal of water, as shown in Scheme 3.

3.2. Linear Absorption, Fluorescence, and Anisotropy Spectra. The linear absorption spectra of SD-FLU-SD and SD compounds are presented in Figure 2a,b with the most

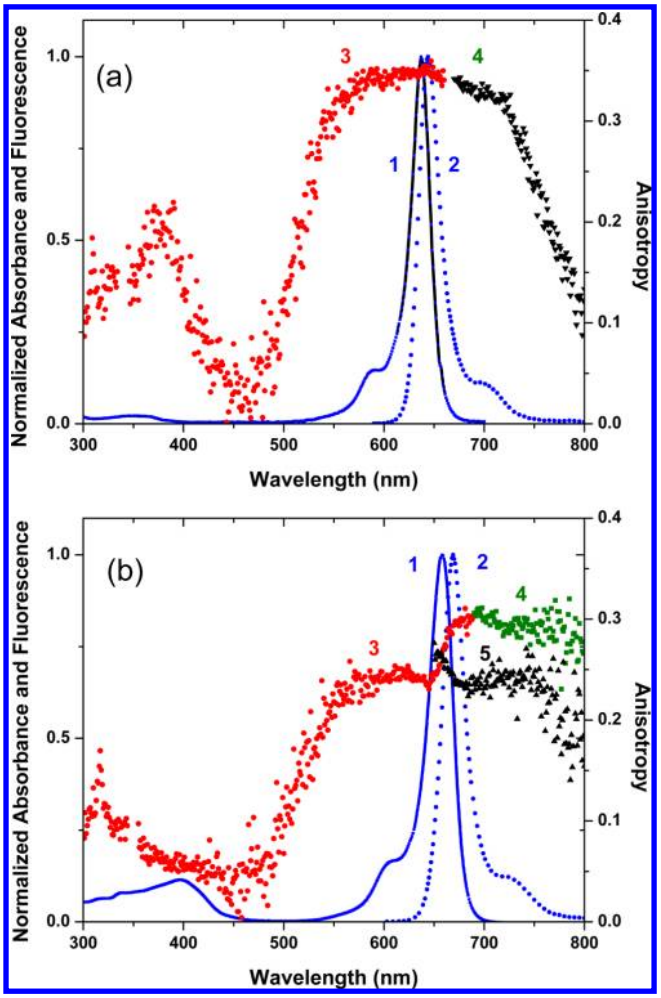

Figure 2. (a) Absorption (1), emission (2), excitation anisotropy (3, measured at fixed emission wavelength 680 nm), and emission anisotropy (4, measured at fixed excitation wavelength 660 nm) spectra for SD in pTHF. (b) Absorption (1), emission (2), excitation anisotropy (3, measured at fixed emission wavelength 700 nm), and emission anisotropy (4, measured at fixed excitation wavelength 680 nm; 5, measured at fixed excitation wavelength 640 nm) spectra for SD-FLU-SD in pTHF.

significant spectroscopic properties listed in Table 2 and Table S1 of the Supporting Information. As shown, the main absorption band of SD (Figure 2a), attributed to the $S_0 \rightarrow S_1$ transition, represents a strong cyanine-like band with a peak at 637 nm (in pTHF) and very weak linear absorption in the visible and UV region corresponding to transitions to higher excited states ($S_0 \rightarrow S_n$). The lowest-lying absorption band of SD-FLU-SD **I** (Figure 2b) in the same solvent exhibited a red shift of ≈20 nm, slightly broader bandwidth, and more intense absorption in the 300−450 nm range. The extinction coefficient (molar absorptivity) of SD-FLU-SD **I** compound was ≈1.7 (in TOL) and ≈1.4 (in DCM and THF) times higher than that for SD **II** itself (see Table 2). The fluorescence spectra of both compounds, SD-FLU-SD **I** and SD **II**, revealed close to mirror-symmetric shapes in all solvents, with a small Stokes shift of 5−10 nm (or 160−200 cm^{-1}), indicating that the excited-state geometry is not significantly modified from the ground-state geometry upon the excitation. Additionally, for SD-FLU-SD **I**, weak fluorescence was observed originating from a higher excited state with a peak position at ≈420 nm (excitation at 350−400 nm). The excitation spectrum of this fluorescence band, in association with the results of quantum chemical calculations (discussed in Quantum Chemical Analysis and Discussion), confirms its link with the FLU constituent. Absorption in the main band and the corresponding fluorescence for both compounds, SD-FLU-SD **I** and SD **II**, show comparatively pronounced vibrational structure related to the skeletal C═C vibrational modes with frequencies of 1200−1300 cm^{-1}.

Fluorescence quantum yields, **Φ**, were measured using the standard method of comparison with a known "red" standard dye, Cresyl Violet perchlorate (Sigma Aldrich) in methanol, which has an absorption peak at 594 nm, fluorescence peak at 620 nm, and a quantum yield of 0.54.[60] To minimize reabsorption effects when measuring fluorescence quantum yields for the molecules having small Stokes shifts, it is important to consider the following: (1) use dilute solutions with optical density at the absorption peak $OD(\lambda^{max}) \leq 0.1$; (2) excite at a wavelength, λ^{exc}, outside the emission band, typically at the blue side of the $S_0 \rightarrow S_1$ band; and (3) to enhance the accuracy of the $OD(\lambda^{exc})$ measurement, this value was recalculated using the ratio between $OD(\lambda^{exc})$ and $OD(\lambda^{max})$ obtained from a reference solution in the same solvent with $OD(\lambda^{max})$ in the optimal range of 1−1.5.

The spectral positions of the optical transitions $S_0 \rightarrow S_n$ and the orientation of the transition dipole moments can be determined using excitation anisotropy measurements.[61] These measurements were performed in viscous polyTHF (pTHF) solutions of average molecular weight ∼650 (Sigma Aldrich, viscosity ∼100−200 cP at 30 °C) to reduce rotational reorientation and at low concentrations (C ≈ 10^{-6} M) to avoid reabsorption of the fluorescence. The excitation anisotropy, defined as $r(\lambda) = [I_{\parallel}(\lambda) - I_{\perp}(\lambda)]/[I_{\parallel}(\lambda) + 2I_{\perp}(\lambda)]$, is measured by recording the emission intensity $I(\lambda)$ at a fixed wavelength, typically near the fluorescence maximum, as a function of excitation wavelength λ at polarizations parallel ($I_{\parallel}(\lambda)$) and perpendicular ($I_{\perp}(\lambda)$) to the excitation polarization.

Table 2. Linear Photophysical Parameters of SD-FLU-SD I and SD II in Three Different Solvents: Absorption (λ^{max}_{abs}) and Fluorescence (λ^{max}_{fl}) Peaks, Maximum Extinction Coefficients (ε^{max}), and Fluorescence Quantum Yields (Φ)

	SD-FLU-SD **I**				SD **II**			
solvent	λ^{max}_{abs} (nm)	ε^{max} (M^{-1} cm^{-1})	λ^{max}_{fl} (nm)	Φ	λ^{max}_{abs} (nm)	ε^{max} (M^{-1} cm^{-1})	λ^{max}_{fl} (nm)	Φ
DCM	656	4.0×10^5	665	0.25 ± 0.04	636	2.8×10^5	644	0.22 ± 0.03
THF	658	4.1×10^5	667	0.31 ± 0.05	637	3.0×10^5	645	0.30 ± 0.05
TOL	661	4.7×10^5	670	0.53 ± 0.08	641	2.8×10^5	648	0.51 ± 0.08

dx.doi.org/10.1021/jp406500t | J. Phys. Chem. C 2013, 117, 23133−23147

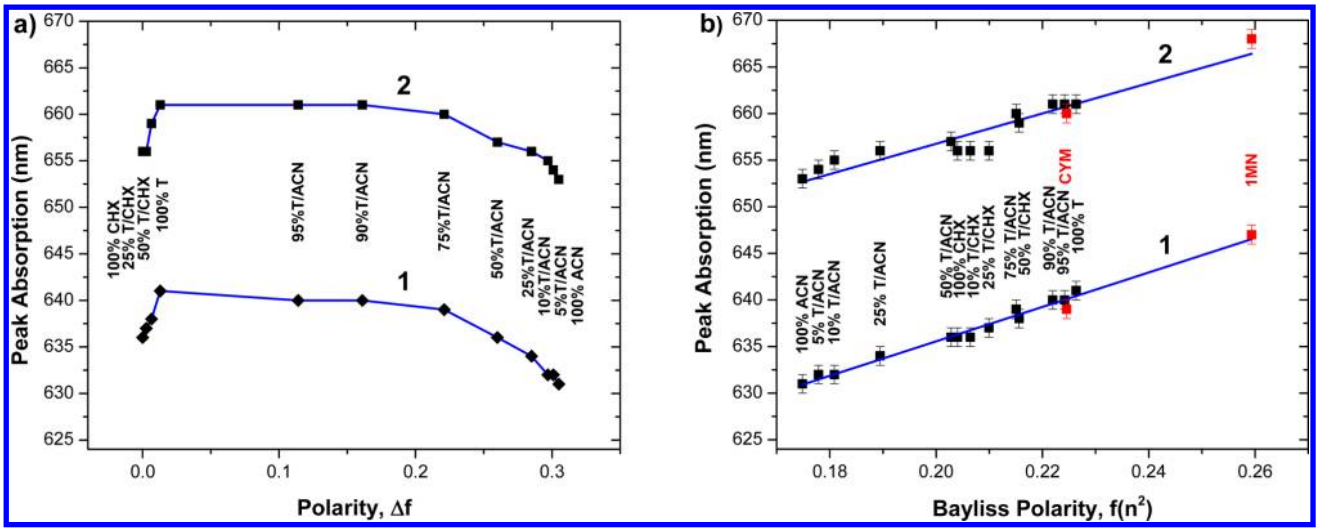

Figure 3. (a) Peak absorption of SD **II** (curve 1) and SD-FLU-SD **I** (curve 2) in TOL/ACN and TOL/CHX mixtures as a function of solvent polarity, Δf. Solid line connecting points is merely a guide for the eye. (b) Peak absorption of SD **II** (1) and SD-FLU-SD **I** (2) in TOL/ACN and TOL/CHX mixtures as a function of Bayliss solvent polarity, $f(n^2)$. Solid lines correspond to correlation coefficients of 0.983 and 0.900 for SD **II** (1) and SD-FLU-SD **I** (2), respectively. Additional aromatic solvents *p*-cymene (CYM) and 1-methylnaphthalene (1MN) are shown in red.

Emission anisotropy can be measured and calculated in the same way; the only difference is that these measurements are performed by fixing an excitation wavelength and tuning the emission wavelength through the fluorescence band. Emission anisotropy provides information about depolarization due to molecular vibrations. First, we analyzed the anisotropy behavior for SD **II**.

As shown in Figure 2a for SD **II**, the excitation anisotropy spectrum, $r(\lambda_{exc})$, measured at the fixed emission wavelength (curve 3), exhibited a sharp increase beginning at ≈500 nm, overlapping smoothly with the emission anisotropy (curve 4, excitation wavelength 660 nm). The emission anisotropy spectrum for SD **II**, $r(\lambda_{em})$, was nearly flat at 650−720 nm and showed a strong depolarization from $r \approx 0.35$ near the peak position at ≈650 nm to $r = 0.1$ at 790 nm because of skeleton vibrational modes. The $r(\lambda_{exc})$ function was constant over the spectral range 550−650 nm (within the $S_0 \rightarrow S_1$ transition) and equaled ≈0.35 (curve 3), indicating nearly parallel orientation of the absorption and emission dipole moments within the main absorption band. In the shorter wavelength region, the anisotropy spectrum of SD **II** was characterized by a broad valley with minimum $r \approx 0$ near ≈450 nm, corresponding to the transition (or group of transitions) forming ≈55° angles with the emission dipole moment.

Next the excitation, $r(\lambda_{exc})$, and emission, $r(\lambda_{em})$, anisotropy spectra of SD-FLU-SD **I** were analyzed, which were essentially different as compared to the anisotropy of SD **II** (Figure 2b, curves 3, 4, and 5). There were a few distinguishing features compared to the anisotropy of SD **II**. First, the $r(\lambda_{exc})$ function (curve 3) was not constant within the main absorption band and exhibited an increase from ≈0.22 to ≈0.3 in the red part of the spectrum ($\lambda_{exc} > 640$ nm), revealing a rather complex nature of the main transition. These changes in the $r(\lambda_{exc})$ function arise from the existence of two electronic transitions within the main absorption band, which can be expected for a double-chromophore structure with a weak interaction between two chromophore subsystems.[62] In the shorter wavelength region, the anisotropy spectrum of SD-FLU-SD **I** displayed a broad valley similar to the $r(\lambda_{exc})$ behavior of SD **II**. Note that the shape of the $r(\lambda_{exc})$ function did not depend on the emission wavelength. Second, the $r(\lambda_{em})$ function (curves 4, 5) strongly depended on the excitation wavelength. As seen in Figure 2b, excitation at the blue (curve 5) and red (curve 4) sides of the main absorption band resulted in different values of $r(\lambda_{em})$: excitation at the red edge led to a higher anisotropy value, $r \approx 0.3$, smoothly overlapping with the corresponding excitation anisotropy function. Third, significant depolarization was not observed within the entire emission range, in contrast to the behavior of SD **II** emission anisotropy.

3.3. Fluorescence Lifetimes. Table 1 lists the experimental lifetimes, radiative lifetimes (calculated by the Birks−Dyson equation[57]), and calculated fluorescence lifetimes. Fluorescence decay curves for SD-FLU-SD **I** and SD **II** in three solvents are shown in Figure S2a,b in the Supporting Information. SD-FLU-SD **I** in DCM showed a double-exponential decay, with a small contribution (≈20%) of the second (slower) component. A weak long-lived component of the fluorescence emission of SD-FLU-SD in DCM presumably can be explained by a small amount of specifically solvated conformers formed in the ground state. All other decays show typical single-exponential character. As shown in Table 1, the calculated and experimental lifetimes for SD in all solvents agree within 20% error (≈30% for THF). For SD-FLU-SD **I** the difference in lifetimes (approximately double) is associated with the existence of two overlapping electronic transitions within the main absorption band, as discussed in Synthesis of SD-FLU-SD (I) and the Symmetrical Squaraine SD (II).

3.4. Polarity Dependence. Spectral positions of the absorption−fluorescence peaks and quantum yields of SD-FLU-SD **I** and SD **II** exhibit a strong dependence on solvent polarity (or orientational polarizability), given by $\Delta f = (\varepsilon - 1)/(2\varepsilon + 1) - (n^2 - 1)/(2n^2 + 1)$ where ε is the static dielectric constant and n is the refractive index of the solvent.[63] Therefore, we performed a detailed investigation of the polarity effects using a selection of solvents and their mixtures with the broadest possible range of Δf values, from nearly zero for CHX to 0.305 for ACN. First, we investigated the polarity effects in mixtures of TOL and ACN with continuously changing solvent polarity in the 0.013−0.306 range. When we extended this range to near zero values, using mixtures of TOL and CHX, the

dx.doi.org/10.1021/jp406500t | J. Phys. Chem. C 2013, 117, 23133−23147

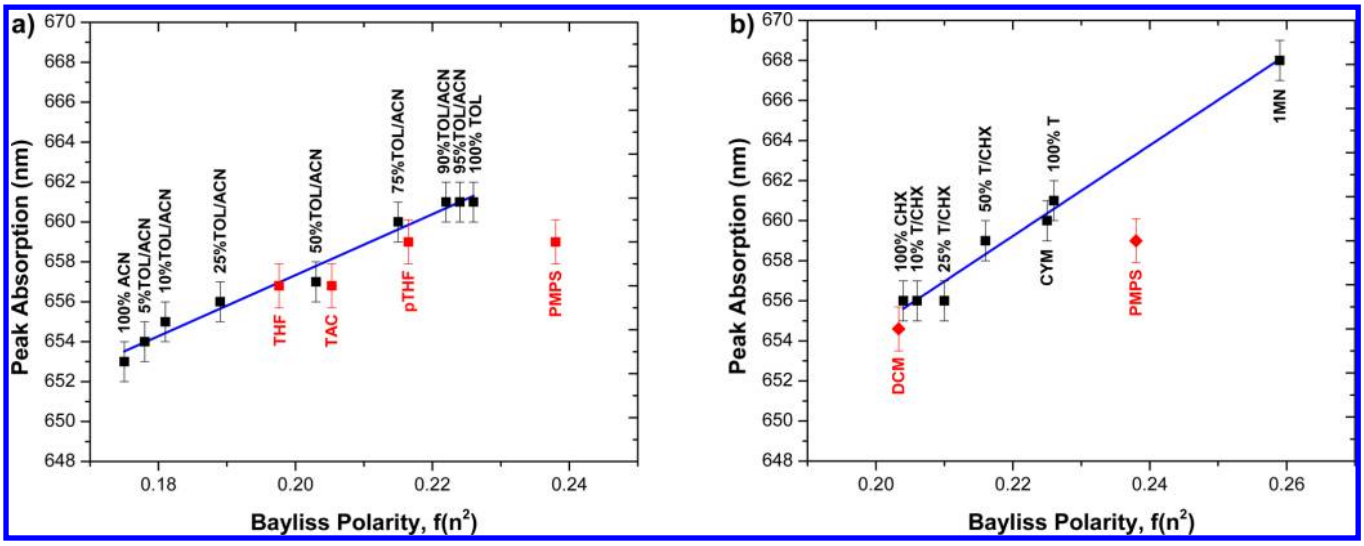

Figure 4. (a) Linear fit of SD-FLU-SD **I** in TOL/ACN mixtures (solid line) and (b) linear fit of SD-FLU-SD **I** in TOL/CHX/aromatic solvent systems (solid line).

reverse trend in peak absorption was obtained, as shown in Figure 3a. Linear photophysical data for three solvents, DCM, THF, and TOL, are given in Tables 1 and 2. Comprehensive linear solvatochromic photophysical data for all solvents used in this study are provided in Table S1 of the Supporting Information.

The results shown in Figure 3a indicate that in both the CHX/TOL and TOL/ACN solvent systems the absorption maximum has the largest bathochromic shift in 100% toluene. The trend seen in the CHX/TOL mixtures reverses in the TOL/ACN mixtures. This poor correlation with Δf led to a search for an alternative polarity scale that would better correlate with the observed results and therefore better explain the impact that the solvent was having on the photophysical properties of these compounds. The Bayliss polarity scale, given by $f(n^2) = (n^2 - 1)/(2n^2 + 1)$, is based only on the electronic polarizability portion of Δf.[64] Plots of peak absorption with $f(n^2)$ resulted in much better correlations with solvent polarity for these solvent systems, and the correlations improved only when the aromatic solvents *p*-cymene and 1-methylnaphthalene were included, as shown in Figure 3b. Linear fits of the two sets of data resulted in good correlation coefficients of 0.900 and 0.983 for SD-FLU-SD **I** and SD **II**, respectively.

Peak absorption values, measured in several additional solvents, such as DCM, THF, methanol, TAC, polyTHF, DMSO, PDMS, GLY, and PMPS, were added to the SD **II** plot (data from Figure 3b), and the results are shown in Figure S3 of the Supporting Information. Most of the data coincide with a linear fit. However, three of the solvents, PDMS, glycerol, and PMPS, result in peak absorptions that fall distinctly below the general trend seen for the other solvents. The common feature among these solvents is their much higher viscosities, 450 cP or larger. This viscosity-dependent effect may be tentatively attributed to limited solubility in the viscous solvents, resulting in partial aggregation and a blue shift of the absorption band.

Further examination of the absorption data for SD-FLU-SD **I** revealed that correlation coefficients even better than 0.9 could be obtained if all solvents were separated into two groups: the first group based on the TOL/ACN mixtures and the second group based on the TOL/CHX mixtures including aromatic solvents. The results are given in Figure 4a,b.

As observed in Figure 4, this solvent segregation led to an improvement of the correlation coefficient for SD-FLU-SD **I** from 0.9 to 0.98, reflecting a difference in these two groups of solvents. Quantum chemical calculations (Quantum Chemical Analysis and Discussion) suggest that the SD-FLU-SD **I** can exist in three different conformations, and this dual solvatochromic response could be an indication that the different solvent systems favor different equilibrium conformational distributions. Also, it is possible that the SD part of SD-FLU-SD **I** is better solvated by the TOL/ACN system, while the FLU construct, with its very nonpolar 10-carbon alkyl chains, is better solvated by the TOL/CHX/aromatic solvents. It is also interesting to note that the peak absorption in THF, triacetin (TAC), and pTHF correlate best with the TOL/ACN system, while values in DCM correlate best with the other solvents. SD-FLU-SD **I** was not sufficiently soluble in PDMS and glycerol to perform absorption measurements in those solvents. However, in viscous PMPS the result for SD-FLU-SD **I** was the same as that observed for SD **II**, i.e., the peak absorption was well below either series.

It is reasonable that the electronic polarizability, or $f(n^2)$ values, of the solvents may not completely account for the effect of all solvents on these molecules. However, the excellent agreement, shown by the data in Figures 3 and 4 and Figure S3 and Table S1 in the Supporting Information, indicates that the electronic polarizability of the solvent is the predominant effect. Good linear correlations of peak absorption with solvent electronic polarizability have been reported previously for several squaraines, while correlations that include dielectric constant are poor.[65,66] This is consistent with the fact that polarity scales, such as Δf, that include the dielectric constant, cannot be used for centrosymmetric molecules with zero permanent dipole moments and nearly equal quadrupolar moments in the ground and first excited states. In these cases only those relationships based on the solvent refractive index are most appropriate because they better reflect the stabilization of the excited state, which is more polarizable than the ground state.[66,67] This stabilization of the excited state is accomplished by dispersive interactions with the highly polarizable solvent.[65,66] It is important to note that this approach excludes any cases of the specific interactions between the solvent and

dx.doi.org/10.1021/jp406500t | J. Phys. Chem. C 2013, 117, 23133−23147

Table 3. Calculated 1PA and 2PA Properties of 19 Lowest Singlet Excited States for SD-FLU-SD I in DCM, Predicted at TD-DFT Level[a]

transition number	Irr	transition type	energy (eV)	wavelength (nm)	oscillator strength	leading configurations	δ_{2PA} (GM)	i	μ_{0i} (D)	μ_{if} (D)
1	B2	$\pi \rightarrow \pi^*$	2.1 (1.97)	588 (628)	3.8	(H-1 → L+1) + (H → L)	0			
2	A1	$\pi \rightarrow \pi^*$	2.15	576	0.8	(H-1 → L) + (H → L+1)	0			
3	A1	$\pi \rightarrow \pi^*$	2.7	458	0	-(H-1 → L) + (H → L+1)	918	S_1	22.7	5.6
4	B2	$\pi \rightarrow \pi^*$	2.7	457	0	(H-1 → L+1) - (H → L)	0			
5	B1	N → π^*	2.84	436	0	(H-4 → L) + (H-3 → L+1)	0			
6	A2	N → π^*	2.84	436	0	(H-4 → L+1) + (H-3 → L)	0			
7	B2	$\pi \rightarrow \pi^*$	3.14	394	0.6	H-2 → L	<60			
8	B2	$\pi \rightarrow \pi^*$	3.26	379	0.2	H-2 → L+1	1015	S_2	9.8	8.2
9	A1	$\pi \rightarrow \pi^*$	3.28	377	0	H → L+1	8787	S_7	8.7	18.3
10	A1	$\pi \rightarrow \pi^*$	3.35	369	0.03	H-1 → L+2	2977	S_7	8.7	11.2
11	A1	$\pi \rightarrow \pi^*$	3.75	330	0	H-5 → L	4281	S_7	8.66	11.1
12	B2	$\pi \rightarrow \pi^*$	3.77	328	0	H-2 → L+2	3030	S_2	9.8	3.0
13	B2	$\pi \rightarrow \pi^*$	3.82	324	0	H-5 → L+1	<60			
14	A2	N → π^*	3.83	323	0.6	(H-10 → L+1) + (H-9 → L)	0			
15	B1	N → π^*	3.83	323	0.25	(H-10 → L) + (H-9 → L+1)	0			
16	A1	$\pi \rightarrow \pi^*$	3.86	320	0.05	H-7 → L	2542	S_1	22.65	1.39
17	B2	$\pi \rightarrow \pi^*$	3.88	318	0.1	H-7 → L+1	0			
18	A1	$\pi \rightarrow \pi^*$	4.05	305	0	H → L+3	8968	S_1	22.65	1.79
19	B2	$\pi \rightarrow \pi^*$	4.14	299	0	H-1 → L+3	4771	S_2	9.75	2.31

[a]Irreducible representation of the final state (symmetry, Irr); excitation energies (eV); 1PA wavelengths (nm); oscillator strengths (proportional to the absorption intensities); leading Kohn-Sham configurations; 2PA cross section (δ_{2PA}); intermediate state in 2PA process (i); transition dipole moments between the ground and intermediate (μ_{0i}) and between the intermediate and final (μ_{if}) states, respectively. FD-DFT values for the first excited state are reported in parentheses.

dye molecules, such as hydrogen bonding or charge-transfer complexes.

4. QUANTUM CHEMICAL ANALYSIS AND DISCUSSION

4.1. Quantum Chemical Approach. Quantum chemical study was performed with the goal of understanding. (1) the formation of the linear absorption spectrum of SD-FLU-SD **I**, (2) polarity effects on the absorption peaks, and (3) the nature of increased 2PA for SD-FLU-SD **I** in comparison with the spectra of the individual SD **II** molecules.

The Gaussian 2009 suite of programs[68] was employed for all density functional theory (DFT) and time-dependent DFT (TD-DFT) calculations. We used a hybrid meta-GGA exchange−correlation functional M05-QX,[69] which is a modified version of the M05 functional[70] with a fraction of the Hartree−Fock exchange increased to 35% to better reproduce both 1PA and 2PA spectra. Excitation energies for polymethine and squaraine (to a lesser extent) dyes are known to present a challenge for the TD-DFT method.[71] The physical reasons for this inaccuracy and a remedy to improve the excitation energy predictions were proposed recently.[72] In sharp contrast with polyenes, the lowest electronic excitation in polymethine dyes results in substantial charge transfer between even and odd atoms in the chain. The TD-DFT method, in commonly used adiabatic approximation, is evaluating the excited-state energy in the potential, generated by the ground state. This approximation works well when the electron density does not change much upon excitation, but results in larger than usual errors in cases where the density of the excited state substantially differs from that of the ground state. However, the electron density of the excited state can be used in a static DFT calculation to obtain a more accurate energy of this excited state, and this approach is called frozen density approximation.[72]

The respective excitation energy can be obtained as a difference (Δ) of the self-consistent field (SCF) energies of the ground- and excited-state determinants (this is known as ΔSCF), or using SCF for the ground state and frozen density for excited state (FD-DFT). These FD-DFT excitation energies for the lowest singlet state are reported in Table 3. The energies for the higher excited states, which are not associated with the substantial changes in electron density, were not corrected.

In our calculations, solvent was taken into account with the polarizable continuum model (PCM) in its recent solvent model density (SMD) parametrization.[73] The ground-state geometries of the investigated dyes were optimized at the M05-QX/6-31G*/PCM theory level, and the vertical electronic transitions were predicted in this geometry using TD-DFT at the TD-M05-QX/6-31G*/PCM theory level. The emission spectra were predicted at the respective optimized geometries of the excited states. The nonequilibrium version of the solvent model was used in absorption prediction, while an equilibrium-state-specific solvation model was used in predicting emission. This means that the solvent polarity, presented by the equation $\Delta f = (\varepsilon - 1)/(2\varepsilon + 1) - (n^2 - 1)/(2n^2 + 1)$, is described by two dielectric constants corresponding to two terms in this equation: the slow component, related to the static dielectric constant and originating from the orientational relaxation of solvent molecules, and the fast component, related to the refractive index and describing the electronic response of the solvent.

In the nonequilibrium solvent model, the ground and excited states are initial and final states, respectively. The electronic component is presumed to instantly adapt to the charge distribution in the final (excited) state of solute, while the orientational component is responding to the charge distribution in the initial (ground) state of solute. In the

dx.doi.org/10.1021/jp406500t | J. Phys. Chem. C 2013, 117, 23133−23147

equilibrium model, the ground and excited states reverse roles and become the final and initial states, respectively. The standard equilibrium solvent model is typically used to simulate fluorescence. In our systems, this model predicted unrealistically large solvatochromic shifts,; therefore, we applied a state-specific solvation method. In this method the external iterations are used to make solvent response self-consistent with the density of the specific excited state.

4.2. Ground-State Conformations of SD-FLU-SD I and Linear Absorption Spectra. SD-FLU-SD **I** has two acetylene bridges that are characterized by low energy rotational barriers. Indeed, the relaxed twist around each of the triple bonds produced a barrier close to 1.0 kcal/mol, while a simultaneous twist of both triple bonds is associated with a barrier of 2.0−2.3 kcal/mol, depending on the solvent. The barriers in the $\pi\pi^*$ excited state are slightly higher, up to 3.2 kcal/mol. The planar geometry of SD-FLU-SD **I** has three possible conformations: up−up, up−down, and down−down, as shown in Figure 5. The angles between transition dipoles of SD and FLU chromophores are ≈59° for up−up, ≈22° for up−down, and ≈70° for down−down conformations.

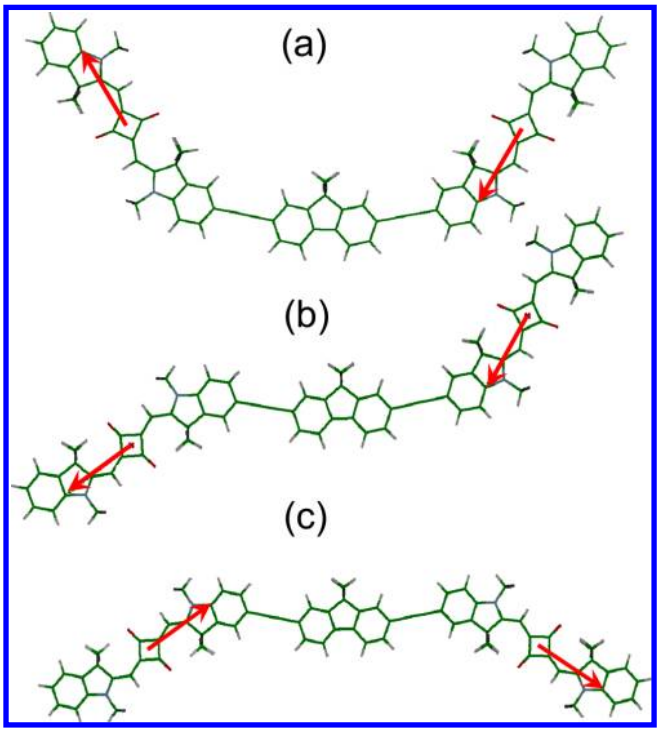

Figure 5. Lowest energy conformers for SD-FLU-SD: (a) up−up, (b) up−down, and (c) down−down.

The ground-state energies of these conformations are very close, differing by only ≈0.1 kcal/mol; therefore, all rotamers about triple bonds coexist in solution in dynamic equilibrium. Our calculations show that three representative rotamers (depicted in Figure 5) are characterized by almost identical linear and 2PA spectra, except for the ratio between the oscillator strength for $S_0 \rightarrow S_1$ and $S_0 \rightarrow S_2$ transitions. However, the energy splitting between these transitions is small, ≈10−20 nm, and cannot be resolved experimentally. Thus, for simplicity, we consider only the down−down conformer in detail.

The shapes of the essential MOs for SD-FLU-SD **I** are presented in Figure 6 while the Gaussian-widened linear absorption spectrum in DCM is shown in Figure 7.

From the analysis of Figures 6 and 7 and Table 3, one can see that the long wavelength absorption band for SD-FLU-SD **I** includes two electronic transitions, $S_0 \rightarrow S_1$ and $S_0 \rightarrow S_2$, as a result of the interaction (coupling) of two squaraine chromophores. These transitions are overlapping because the splitting energy is small (≈15 nm), and there is a 5-fold difference in their oscillator strengths. The transition dipole for $S_0 \rightarrow S_1$ is parallel to the long molecular axis, while the transition dipole for $S_0 \rightarrow S_2$ is smaller and perpendicular to it. The leading configurations involved in these transitions, H → L, H-1 → L, H → L+1, and H-1 → L+1 are localized within squaraine fragments. Results of calculations are in agreement with the excitation anisotropy data shown in Figure 2. The two next transitions with zero oscillator strengths involve the same configurations and represent forbidden transitions into the second excited state for each squaraine chromophore. Transitions 5 and 6 are of the N → π^* nature, which is due to the existence of unshared electron pairs on the oxygen atoms, and are characterized by zero oscillator strength. They involve H-3 and H-4 molecular orbitals (see Figure 6), which are localized in the plane perpendicular to the main $\pi \rightarrow \pi^*$ conjugation system.

The next group of the "bright" transitions is placed in the spectral range 370−400 nm and involve almost "pure" transitions from H-2 to L and L+1. They represent the charge-transfer transitions from the fluorene fragment (H-2) to squaraine parts (L and L+1). $S_0 \rightarrow S_{14}$ and $S_0 \rightarrow S_{15}$ transitions are of n → π^* nature, involving H-9 and H-10 molecular orbitals, which are not shown in Figure 6. Transitions, placed in the range of 330 nm, are of the $\pi \rightarrow \pi^*$ nature and are confined mainly within the fluorene fragment (from H-2 to L+2).

4.3. Analysis of the 1PA and 2PA Spectra. Calculated and experimental 1PA and 2PA spectra for SD **II** and SD-FLU-SD **I** in DCM are shown in Figures 7 and 8 with the 2PA spectra plotted on a semilogarithmic scale. For comparison of transition wavelengths, 1PA and 2PA spectra for each dye are shown on the same graph with separate axes for 1PA (bottom) and 2PA (top) photon wavelengths.

One can see from these figures that the calculated and experimental 1PA spectra are in general agreement despite some differences (note that we did not attempt to adjust any parameters to get a complete overlap). The position of maximum absorption wavelengths was predicted nearly 20 nm shorter than experimental values for the reasons discussed above. Apparently, FD-DFT reduces this disagreement but does not eliminate it completely. The higher-lying bright states are predicted close to the experimental maxima, but they are somewhat too sharp. This is expected from a calculation not taking into account vibronic broadening. The calculated line shapes appear because of the use of habitual empirical line width of 0.1 eV and are approximate.

The experimentally observed 2PA spectrum of SD **II** (see Figure 8) consisted of two bands: a relatively weak peak of $\delta_{2PA} \approx 50$ GM at 600 nm, corresponding to the 2PA excitation into the vibronic shoulder of the strongly one-photon-allowed $S_0 \rightarrow S_1$ transition, and a high intensity band with δ_{2PA} up to 7200 GM (two-photon excitation at 700 nm). The peak of this band is not resolved experimentally because of the tail of the linear absorption. It is important to note that there is a region between these two 2PA bands where the 2PA cross section dips

dx.doi.org/10.1021/jp406500t | J. Phys. Chem. C 2013, 117, 23133−23147

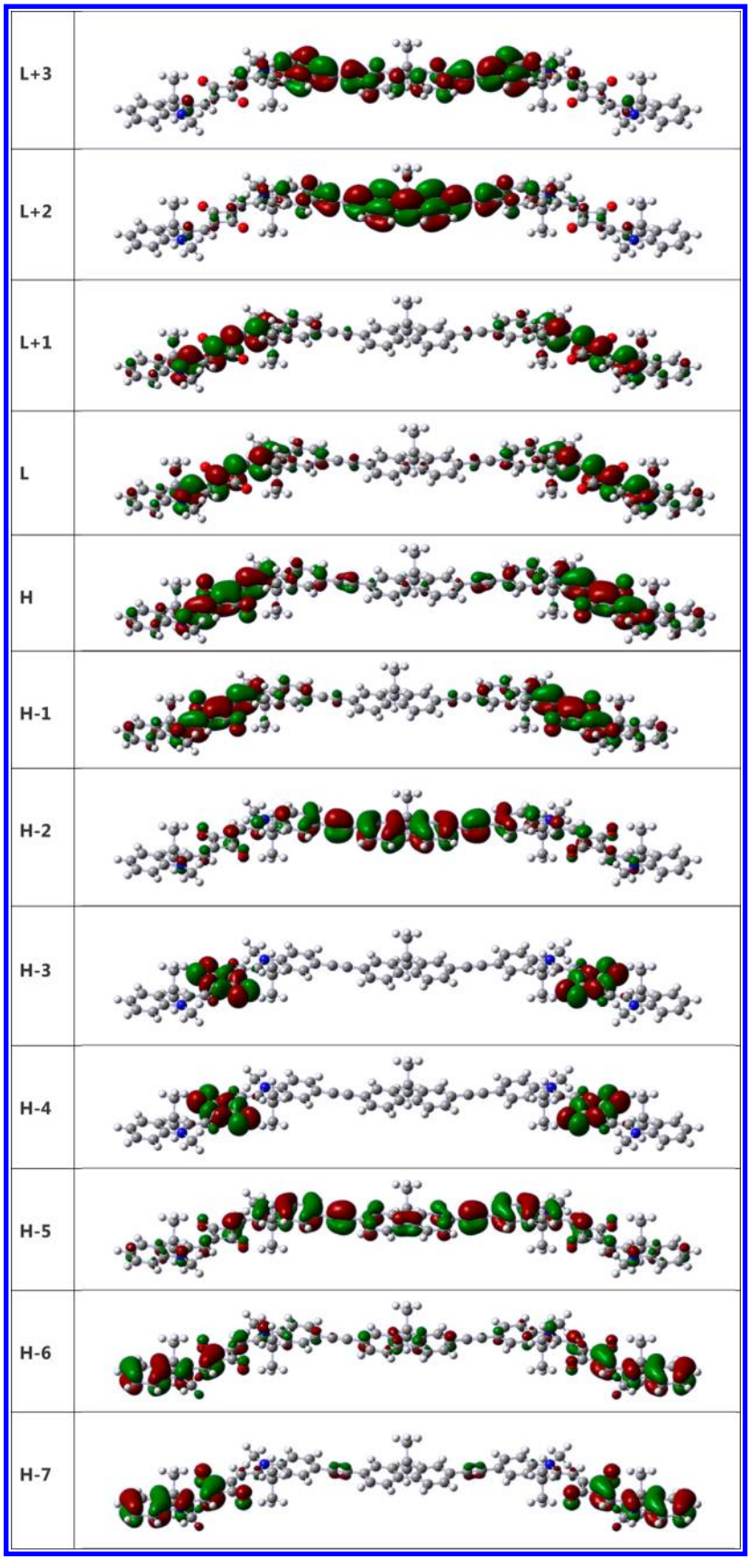

Figure 6. Shapes of the HOMO (H), LUMO (L), and other essential Kohn−Sham orbitals involved in the main electronic transitions in SD-FLU-SD.

dx.doi.org/10.1021/jp406500t | J. Phys. Chem. C 2013, 117, 23133−23147

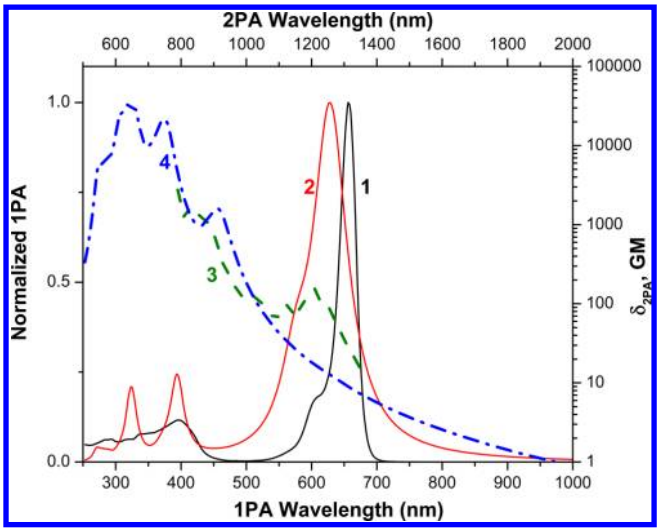

Figure 7. Calculated and experimental 1PA and 2PA spectra for SD-FLU-SD **I** in DCM: (1) experimental 1PA; (2) calculated 1PA; (3) measured 2PA; (4) calculated 2PA.

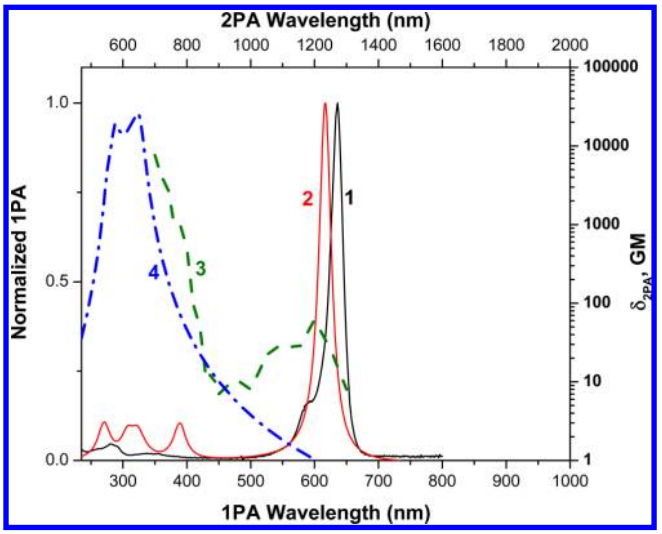

Figure 8. Calculated and experimental 1PA and 2PA spectra for SD **II** in DCM: (1) experimental 1PA; (2) calculated 1PA; (3) measured 2PA; (4) calculated 2PA.

to very small values (≈5−7 GM). The calculations predict the short wavelength 2PA band to peak at ≈600 nm, in good agreement with the trend on the experimental spectrum. The magnitudes of predicted and observed δ_{2PA} values are also in a good agreement.

Because the vibronic effects are not included in our calculations and purely electronic transition into S_1 has a vanishing 2PA cross section, only the tail of the calculated electronic 2PA band was observed in the long wavelength region. The nature of the 2PA bands for SD **II** has been investigated previously.[19,21,55,74] As was shown in ref 55, there are four 2PA bands measured for SD **II**:

1. A weak band at the 2PA into the vibronic shoulder of the 1PA band with $\delta_{2PA} \approx 40$ GM. By dipole selection rules this band is 2PA forbidden, but Scherer et al.[21] found that this band is weakly allowed because of vibronic coupling. Fu et al.[19] confirmed this finding via 2PA anisotropy measurements. Brédas et al.[74] also confirmed this finding through quantum calculations and by ruling out the possibility that this 2PA band is due to either electronic transitions into the 1PA bands of possible noncentrosymmetric conformers or excitation into the S_2 electronic state with the energy close to the 1PA band.
2. The first two-photon allowed band around 1100 nm (2PA excitation) into S_2 state.
3. The more intense 2PA allowed band at 820 nm (2PA excitation). Scherer et al.[21] reported this 2PA band and demonstrated, by polarized light measurements, that this band is due to an A_g-A_g transition.
4. The highest intensity 2PA band at 710 nm (2PA excitation) with $\delta_{2PA} \approx 5200$ GM, the maximum of this band being unreachable because of the tailing of the 1PA band.[19,55]

The experimental 2PA spectrum for the SD-FLU-SD is presented in Figure 7. It is broader than that of SD **II** and covers the entire measurable region with δ_{2PA} ranging from 150 GM (two-photon excitation at ≈1200 nm) to 3000 GM (two-photon excitation at ≈800 nm). The calculated 2PA spectrum again is missing the vibronic shoulder of S_1 and finds two peaks at 750 and 650 nm, just outside the experimentally accessible region. Our study suggests that the broadening of the 2PA in SD-FLU-SD **I**, as compared to that of the SD **II** spectrum, can be explained by the existence of several efficient CT bands across the large conjugated chain via alkyne triple bonds from the SD to the FLU constituents.

To understand the nature of the 2PA transitions in SD-FLU-SD **I**, we present the calculated properties of 19 lowest singlet excited states in Table 3. One can see that the first calculated 2PA band with δ_{2PA} of 918 GM is placed at 458 nm (two-photon excitation at 916 nm) and corresponds to S_3 final state with S_1 as intermediate state. The Kohn−Sham orbitals involved in this transition are localized within the squaraine fragments only (H and H-1 to L and L+1). The next group of the overlapping 2PA transitions (to final S_9, S_{10}, S_{11} states) is predicted in the range 330−377 nm (two-photon excitation 650−750 nm). They involve the higher 1PA active state, S_7 as the intermediate state (these transitions are localized on FLU fragment). Close to these states are 2PA-active S_8 and S_{12} states that have S_2 as an intermediate state. State S_2, along with S_1, originate from the coupling of HOMO-to-LUMO transitions of

Table 4. Predicted Solvatochromic Shifts ($\Delta\lambda_{abs}$ and $\Delta\lambda_{fl}$) for SD and SD-FLU-SD in CHX, TOL, and DCM and the Potential Barrier (ΔE) to Radiationless Deactivation; The Orientational (ε) and Electronic (ε_{inf}) Dielectric Constants of the Solvents Used in Nonequilibrium PCM Model

	ε	ε_{inf}	SD $\Delta\lambda_{abs}$ (nm)	SD $\Delta\lambda_{fl}$ (nm)	SD ΔE (kcal mol^{-1})	SD-FLU-SD $\Delta\lambda_{abs}$ (nm)	SD-FLU-SD $\Delta\lambda_{flu}$ (nm)
VAC	1.000	1.000	0	0	7.2	0	0
CHX	2.017	2.035	41	41	1.2	36	36
TOL	2.374	2.238	46	50	4.2	40	44
DCM	35.688	1.807	36	36	1.4	32	90

dx.doi.org/10.1021/jp406500t | J. Phys. Chem. C 2013, 117, 23133−23147

the two SD fragments placed at an angle. While the $S_0 \rightarrow S_1$ transition dipole is parallel to the long molecular axis, the $S_0 \rightarrow S_2$ transition dipole is perpendicular to it (while still within the molecular plane). These last groups of 2PA states represent mainly CT transitions from the orbitals localized on fluorene (H-2 and H-5) to those localized on squaraine (L and L+1) fragments. Similar CT transitions (H → L+3) are responsible for the next group of intensive 2PA transitions, which are not experimentally accessible. It is worth noting that the two-dimensional nature of the combined chromophore SD-FLU-SD **I** plays an important role in 2PA absorption. It involves more states in the 2PA process by making more 1PA active states available as intermediate states.

4.4. Solvatochromic Shifts and Solvent Dependence of the Quantum Yield. The polarizable continuum model predicts solvatochromic shifts in both SD **II** and SD-FLU-SD **I** in close agreement with the experiment, as one can see from Table 4. In order to understand the reversed direction of solvatochromic shift in CHX/TOL and TOL/ACN mixtures (shown in Figure 3a), we analyzed the polarity of SD **II** solute in the ground and excited states in polar and nonpolar solvents. Our analysis reveals that while the dipole moments of solutes are zero, the molecular quadrupole moments and Mulliken atomic charges (not shown) are very similar in the ground and excited states, although they somewhat differ from one solvent to another. In conjunction with the nonequilibrium PCM model, employed in our simulations, this means that the slow (orientational) component of the solvent reaction field stabilizes the ground and excited states to the same degree and does not effect a solvatochromic shift. The fast (electronic) solvent response, however, stabilizes the excited state only. Therefore, solvatochromic shifts are determined by the dielectric constant at the high-frequency limit (defined as the square root of the refractive index). Hence, solvatochromic shifts appear monotonic according to the Bayliss solvent polarity scale, in full agreement with the experimental data presented in Figure 3b. Emission solvatochromism follows a similar trend, except this time it is the final ground state that experiences the extra stabilization by the fast component of the solvent reaction field.

To simulate the emission from SD **II** and SD-FLU-SD **I**, we optimized the geometry of the S_1 excited state into the local minimum near the Franck–Condon region. However, as has been known, many donor–acceptor substituted chromophores often demonstrate another global minimum referred to as a twisted intramolecular charge-transfer (TICT) state.[66,75−78] We optimized SD **II** in the ground and first excited states with one dihedral constraint and plotted the minimal energy pathways (MEP) upon change of the dihedral angle from the planar *trans*- (0°) through *twist*- (90°) to the *cis*- conformation (180°). These MEPs are shown in Figure S4b–e of the Supporting Information. As anticipated, the ground state in a vacuum has a global minimum for the *trans*-conformation (Figure S4b) and another (2.5 kcal/mol less stable) minimum for the *cis*-conformation (Figure S4e). They are separated by a ∼23 kcal/mol barrier at an 80° twist (Figure S4d). Also expected, this dihedral rotation is accompanied by the pyramidalization of both carbon atoms separated by the rotating bond. Upon this twist, the dipole moment of the ground state increased gradually from 0.3 to 3.0 D then jumped abruptly to 11 D and retained this value in the dihedral range (60–120°). This jump indicates the transition from diradical to zwitterionic nature of the twisted conformation, consistent with the charge-transfer state. The solvent stabilizes the twisted zwitterion, reducing the barrier to 21–22 kcal/mol, but retains MEP unchanged otherwise.

The excited-state MEP is distinctly different. The first excited state retains high oscillator strengths and closely follows the ground-state MEP and the dipole moment for the first few steps from the planar conformation (0–20° and 140–180°). However, after the next step away from planarity, the permanent dipole moment increased sharply, the oscillator strength vanished, and MEP descended to a global minimum at an 80° twist. The excited-state energy in the twisted conformation was nearly degenerate to the ground state at the same geometry, and the value of the dipole moment was similar to that in zwitterionic ground state, while the direction is opposite. This situation is similar to the sudden polarization (spontaneous symmetry breaking) of the ethylene molecule and its transitions to a zwitterionic form upon intramolecular twist.[79]

Near degeneracy of the ground and excited states in twisted conformation opens an efficient channel for radiationless deactivation of the excited state, and the apparent fluorescence quantum yield depends on the ratio of the emission rate and the conformational transition over the potential barrier at a 30° twist. Seemingly, this barrier is the crossing point between the ascending MEP of the diradical bright excited state and the descending MEP of another (zwitterionic) dark charge-transfer state. The solvent has a critical effect on the height of this barrier. As one can see from Figure S4a of the Supporting Information, in a vacuum this barrier is relatively high (7.2 kcal/mol); in TOL, it is reduced to 4.2 kcal/mol, while in CHX and ACN it is much smaller (1.2 and 1.4 kcal/mol, respectively). This trend is similar to the trend in solvatochromic shift, which was discussed earlier, i.e., the value is determined primarily by fast (electronic) solvent polarity character.

5. CONCLUSIONS

A new hybrid squaraine–fluorene–squaraine dye has been designed to absorb over a broad range of wavelengths and synthesized by coupling two squaraine dyes to a central fluorene via ethyne linkages. The linear and two-photon absorption properties of the dye were measured and compared with the photophysical properties of the corresponding squaraine constituent. Extensive solvatochromic characterization was also conducted. Quantum chemical calculations were used to enhance understanding of the experimentally measured 1PA and 2PA spectra, the fluorescence quantum yields, and solvatochromism leading to the following conclusions.

1. The long wavelength absorption band of SD-FLU-SD is the result of $S_0 \rightarrow S_1$ and $S_0 \rightarrow S_2$ transitions due to the coupling of squaraine fragments, but they are too close in energy to be resolved experimentally. This result agrees with excitation anisotropy measurements. Two additional transitions within the squaraine fragments reveal similar splitting but have zero oscillator strengths because they are forbidden transitions into the second excited state of the squaraine segments.
2. The next higher transitions with nonzero oscillator strengths are in the 370–400 nm range and involve a large fraction of charge transfer from the fluorene to squaraine fragments.

dx.doi.org/10.1021/jp406500t | J. Phys. Chem. C 2013, 117, 23133−23147

3. A third group of transitions near 300 nm are transitions within the fluorene moiety.

The experimentally measured 2PA spectrum for SD-FLU-SD **I** was broader than that of SD **II**, with δ_{2PA} ranging from 150 GM to 3000 GM over the wavelength range from 1200 to 800 nm 2PA excitation. Quantum chemical calculations indicate that this broadening is a result of several efficient charge-transfer transitions across the ethyne bridges between fluorene and squaraine components. Four groups of 2PA transitions are predicted as described below.

(a) A 2PA band with a cross section of 918 GM is at 458 nm (2PA excitation at 916 nm). This corresponds to an S_3 final state with S_1 as intermediate state occurring on squaraine constructs only.
(b) A group of overlapping transitions in the 330−377 nm range (2PA excitation 650−750 nm) is located on the fluorene moiety. These involve final states S_9, S_{10}, and S_{11} with 1PA active S_7 intermediate state.
(c) Next are transitions involving 2PA active S_8 and S_{12} states, with S_2 and S_1 as intermediates. These involve the coupling of transitions on the two squaraine fragments oriented at an angle to each other.
(d) The highest energy 2PA states are the result of charge-transfer transitions from fluorene to squaraine chromophore units.
(e) A fifth group of predicted high-intensity 2PA transitions is also due to charge-transfer transitions, but these transitions are not experimentally observable.

Detailed studies of the solvatochromic properties of SD **II** and SD-FLU-SD **I** revealed that solvatochromic shifts were opposite in direction in the two solvent systems, CHX/TOL and TOL/ACN. The polarizable continuum model predicts solvatochromic shifts in good agreement with experiment. It was found that the slower orientational component of the solvent polarity stabilizes the ground and excited states equally and therefore does not have an impact on the measured solvatochromic shifts. The faster electronic polarizability of the solvent stabilizes the excited state only. This helps explain the good correlations between solvatochromic shifts and the Bayliss solvent polarity scale, which includes only the solvent refractive index when calculating solvent polarity. Emission solvatochromism was found to experimentally follow a trend that was the same as that of absorption. In this case it is the ground state that is more highly stabilized by the electronic polarizability of the solvent.

The fluorescence quantum yields were found to follow the trend observed in solvatochromic shifts with opposite directions for the two solvent systems, CHX/TOL and TOL/ACN. The quantum chemical calculations found that conformational transition into a twisted intramolecular charge-transfer (TICT) state is highly competitive with the emission process from the planar Franck−Condon state. This conformational transition opens an efficient nonradiative deactivation channel, and the height of the barrier leading to TICT primarily determines the fluorescence quantum yield in different solvents.

Results obtained in the study of SD-FLU-SD **I** and its SD **II** model demonstrate the successful design strategy for the optical material with broad-range 2PA absorption. The integrated experimental and theoretical approach provides a comprehensive understanding of structure−property relationships required for efficient two-photon absorbing materials as well as the influence of solvents on the observed spectral properties of these compounds. This study provides a foundation for the future design of new photonic materials for a range of potential chemical, biological, and optical applications.

■ ASSOCIATED CONTENT

Supporting Information

Complete synthetic procedures, ^{1}H and ^{13}C NMR spectra, complete photophysical and solvatochromic summary data, and additional information. This material is available free of charge via the Internet at http://pubs.acs.org.

■ AUTHOR INFORMATION

Corresponding Author

*Department of Chemistry, University of Central Florida, P.O. Box 162366, Orlando, FL 32816. Phone: 407-823-2566. E-mail: belfield@ucf.edu.

Notes

The authors declare no competing financial interest.

■ ACKNOWLEDGMENTS

We acknowledge the National Science Foundation (ECCS-0925712, CHE-0840431, and CHE-0832622), the US National Academy of Sciences (PGA-P210877), and the National Academy of Sciences of the Ukraine (Grants 1.4.1.B/153 and VC/157). We thank Dr. David Richardson of the University of Central Florida Chemistry Department for assistance with 2D NMR measurements of SD-FLU-SD **I**.

■ REFERENCES

(1) Andrade, C. D.; Yanez, C. O.; Rodriguez, L.; Belfield, K. D. A Series of Fluorene-Based Two-Photon Absorbing Molecules: Synthesis, Linear and Nonlinear Characterization, and Bioimaging. *J. Org. Chem.* **2010**, *75*, 3975−3982.
(2) Morales, A. R.; Yanez, C. O.; Schafer-Hales, K. J.; Marcus, A. I.; Belfield, K. D. Biomolecule Labeling and Imaging with a New Fluorenyl Two-Photon Fluorescent Probe. *Bioconjugate Chem.* **2009**, *20*, 1992−2000.
(3) Pu, K.-Y.; Li, K.; Liu, B. A Molecular Brush Approach to Enhance Quantum Yield and Suppress Nonspecific Interactions of Conjugated Polyelectrolyte for Targeted Far-Red/Near-Infrared Fluorescence Cell Imaging. *Adv. Funct. Mater.* **2010**, *20*, 2770−2777.
(4) Wang, X.; Nguyen, D. M.; Yanez, C. O.; Rodriguez, L.; Ahn, H.-Y.; Bondar, M. V.; Belfield, K. D. High-Fidelity Hydrophilic Probe for Two-Photon Fluorescence Lysosomal Imaging. *J. Am. Chem. Soc.* **2010**, *132*, 12237−12239.
(5) Kumi, G.; Yanez, C. O.; Belfield, K. D.; Fourkas, T. High-Speed Multiphoton Absorption Polymerization: Fabrication of Microfluidic Channels with Arbitrary Cross-Sections and High Aspect Ratios. *Lab Chip* **2010**, *10*, 1057−1060.
(6) Yang, B. L.; Cho, N.; Joo, D.-L.; Lee, K.-S.; Son, Y.; Yang, D.-Y. Synthesis and Characterization of Two-Photon Absorbing Dithienothiophene Derivative with Silyl End Group. *Mol. Cryst. Liq. Cryst.* **2008**, *491*, 173−182.
(7) Corredor, C. C.; Huang, Z.-L.; Belfield, K. D.; Morales, A. R.; Bondar, M. V. Photochromic Polymer Composites for Two-Photon 3D Optical Data Storage. *Chem. Mater.* **2007**, *19*, 5165−5173.
(8) Belfield, K. D.; Corredor, C. C.; Morales, A. R.; Dessources, M. A.; Hernandez, F. E. Synthesis and Characterization of New Fluorene-Based Singlet Oxygen Sensitizers. *J. Fluoresc.* **2006**, *16*, 105−110.
(9) Andrasik, S. J.; Belfield, K. D.; Bondar, M. V.; Hernandez, F. E.; Morales, A. R.; Przhonska, O. V.; Yao, S. One- and Two-Photon Singlet Oxygen Generation with New Fluorene-Based Photosensitizers. *ChemPhysChem* **2007**, *8*, 399−404.

(10) Belfield, K. D.; Bondar, M. V.; Morales, A. R.; Yue, X.; Luchita, G.; Przhonska, O. V.; Kachkovsky, O. D. Two-Photon Absorption and Time-Resolved Stimulated Emission Depletion Spectroscopy of a New Fluorenyl Derivative. *ChemPhysChem* **2012**, *13*, 3481−3491.
(11) Belfield, K. D.; Bondar, M. V.; Yanez, C. O.; Hernandez, F. E.; Przhonska, O. V. One- and Two-Photon Stimulated Emission Depletion of a Sulfonyl-Containing Fluorene Derivative. *J. Phys. Chem. B* **2009**, *113*, 7101−7106.
(12) Feng, X. J.; Wu, P. L.; Tam, H. L.; Li, K. F.; Wong, M. S.; Cheah, K. W. Fluorene-Based π-Conjugated Oligomers for Efficient Three-Photon Excited Photoluminescence and Lasing. *Chem.—Eur. J.* **2009**, *15*, 11681−11691.
(13) Feng, X. J.; Wu, P. L.; Li, K. F.; Wong, M. S.; Cheah, K. W. Highly Efficient Multiphoton-Absorbing Quadrupolar Oligomers for Frequency Upconversion. *Chem.—Eur. J.* **2011**, *17*, 2518−2526.
(14) Belfield, K. D.; Yao, S.; Bondar, M. V. Two-Photon Absorbing Photonic Materials: From Fundamentals to Applications. *Adv. Polym. Sci.* **2008**, *213*, 97−156.
(15) Scherf, U.; List, J. W. Semiconducting Polyfluorenes—Towards Reliable Structure−Property Relationships. *Adv. Mater.* **2002**, *14*, 477−487.
(16) Chung, S.-J.; Zheng, S.; Odani, T.; Beverina, L.; Fu, J.; Padilha, L. A.; Biesso, A.; Hales, J. M.; Zhan, X.; Schmidt, K.; et al. Extended Squaraine Dyes with Large Two-Photon Absorption Cross-Sections. *J. Am. Chem. Soc.* **2006**, *128*, 14444−14445.
(17) Hales, J. M.; Hagan, D. J.; Van Stryland, E. W.; Schafer, K. J.; Morales, A. R.; Belfield, K. D.; Pacher, P.; Kwon, O.; Zojer, E.; Bredas, J. L. Resonance Enhancement of Two-Photon Absorption in Substituted Fluorene Molecules. *J. Chem. Phys.* **2004**, *121*, 3152−3160.
(18) Fu, J.; Padilha, L. A.; Hagan, D. J.; Van Stryland, E. W.; Przhonska, O. V.; Bondar, M. V.; Slominsky, Yu. L.; Kachkovski, A. D. Molecular Structure—Two-Photon Absorption Property Relations in Polymethine Dyes. *J. Opt. Soc. Am. B* **2007**, *24*, 56−66.
(19) Fu, J.; Padilha, L. A.; Hagan, D. J.; Van Stryland, E. W.; Przhonska, O. V.; Bondar, M. V.; Slominsky, Yu. L.; Kachkovski, A. D. Experimental and Theoretical Approaches to Understanding Two-Photon Absorption Spectra in Polymethine and Squaraine Molecules. *J. Opt. Soc. Am. B* **2007**, *24*, 67−76.
(20) Lepkowicz, R. S.; Przhonska, O. V.; Hales, J. M.; Hagan, D. J.; Van Stryland, E. W.; Bondar, M. V.; Slominsky, Yu. L.; Kachkovski, A. D. Femtosecond-to-Nanosecond Nonlinear Spectroscopy of Polymethine Molecules. *J. Opt. Soc. Am. B* **2005**, *22*, 2664−2685.
(21) Scherer, D.; Dorfler, R.; Feldner, A.; Vogtmann, T.; Schwoerer, M.; Lawrentz, U.; Grahn, W.; Lambert, C. Two-Photon States in Squaraine Monomers and Oligomers. *Chem. Phys.* **2002**, *279*, 179−207.
(22) Terenziani, F.; Painelli, A.; Katan, C.; Charlot, M.; Blanchard-Desce, M. Charge Instability in Quadrupolar Chromophores: Symmetry Breaking and Solvatochromism. *J. Am. Chem. Soc.* **2006**, *128*, 15742−15755.
(23) Padilha, L. A.; Webster, S.; Hu, H.; Przhonska, O. V.; Hagan, D. J.; Van Stryland, E. W.; Bondar, M. V.; Davydenko, I. G.; Slominsky, Yu. L.; et al. Excited State Absorption and Decay Kinetics of Near IR Polymethine Dyes. *Chem. Phys.* **2008**, *352*, 97−105.
(24) Lim, J. H.; Przhonska, O. V.; Khodja, S.; Yang, S.; Ross, T. S.; Hagan, D. J.; Van Stryland, E. W.; Bondar, M. V.; Slominsky, Yu. L. Polymethine and Squarylium Molecules with Large Excited-State Absorption. *Chem. Phys.* **1999**, *245*, 79−97.
(25) Lepkowicz, R. S.; Przhonska, O. V.; Hales, J. M.; Hagan, D. J.; Van Stryland, E. W.; Bondar, M. V.; Slominsky, Yu. L.; Kachkovski, A. D. Excited-State Absorption Dynamics in Polymethine Dyes Detected by Polarization-Resolved Pump-Probe Measurements. *Chem. Phys.* **2003**, *286*, 277−291.
(26) Fu, J.; Przhonska, O. V.; Padilha, L. A.; Hagan, D. J.; Van Stryland, E. W.; Belfield, K. D.; Bondar, M. V.; Slominsky, Yu. L.; Kachkovski, A. D. Two-Photon Anisotropy: Analytical Description and Molecular Modeling for Symmetrical and Asymmetrical Organic Dyes. *Chem. Phys.* **2006**, *321*, 257−268.
(27) Webster, S.; Fu, J.; Padilha, L. A.; Przhonska, O. V.; Hagan, D. J.; Van Stryland, E. W.; Bondar, M. V.; Slominsky, Y. L.; Kachkovski, A. D. Comparison of Nonlinear Absorption in Three Similar Dyes: Polymethine, Squaraine, and Tetraone. *Chem. Phys.* **2008**, *348*, 143−151.
(28) Beverina, L.; Salice, P. Squaraine Compounds: Tailored Design and Synthesis Towards a Variety of Material Science Applications. *Eur. J. Org. Chem.* **2010**, 1207−1225.
(29) Ajayaghosh, A. Chemistry of Squaraine-Derived Materials: Near-IR Dyes, Low Band Gap Systems, and Cation Sensors. *Acc. Chem. Res.* **2005**, *38*, 449−459.
(30) Das, S.; Thomas, K. G.; George, M. V. Photophysical and Photochemical Properties of Squaraines in Homogeneous and Heterogeneous Media. *Mol. Supramol. Photochem.* **1997**, *1*, 467−517.
(31) Sreejith, S.; Carol, P.; Chithra, P.; Ajayaghosh, A. Squaraine Dyes: A Mine of Molecular Materials. *J. Mater. Chem.* **2008**, *18*, 264−274.
(32) Terpetschnig, E.; Lakowicz, J. R. Synthesis and Characterization of Unsymmetrical Squaraines: A New Class of Cyanine Dyes. *Dyes Pigm.* **1993**, *21*, 227−234.
(33) Terpetschnig, E.; Szmacinski, H.; Lakowicz, J. R. Synthesis, Spectral Properties and Photostabilities of Symmetrical and Unsymmetrical Squaraines; A New Class of Fluorophores with Long-Wavelength Excitation and Emission. *Anal. Chim. Acta* **1993**, *282*, 633−641.
(34) Law, K. Y. Organic Photoconductive Materials: Recent Trends and Developments. *Chem. Rev.* **1993**, *93*, 449−486.
(35) Piechowski, A.; Bird, G.; Morel, D.; Stogryn, E. Desirable Properties of Photovoltaic Dyes. *J. Phys. Chem.* **1984**, *88*, 934−950.
(36) Yum, J.-H.; Walter, P.; Huber, S.; Rentsch, D.; Geiger, T.; Nuesch, F.; De Angelis, F.; Gratzel, M.; Nazeeruddin, M. K. Efficient Far Red Sensitization of Nanocrystalline TiO_2 Films by an Unsymmetrical Squaraine Dye. *J. Am. Chem. Soc.* **2007**, *129*, 10320−10321.
(37) Xiang, Z.; Nesterov, E. E.; Skoch, J.; Lin, T.; Hyman, B. T.; Swager, T. M.; Bacskai, B. J.; Reeves, S. A. Detection of Myelination Using a Novel Histological Probe. *J. Histochem. Cytochem.* **2005**, *53*, 1511−1516.
(38) Das, S.; Thomas, K. G.; Thomas, K. J.; Kamat, P. V.; George, M. V. Photochemistry of Squaraine Dyes. 8. Photophysical Properties of Crown Ether Squaraine Fluoroionophores and Their Metal Ion Complexes. *J. Phys. Chem.* **1994**, *98*, 9291−9296.
(39) Smits, E. C. P.; Setayesh, S.; Anthopoulos, T. D.; Buechel, M.; Nijssen, W.; Coehoorn, R.; Blom, P. W. M.; de Boer, B.; de Leeuw, D. M. Near-Infrared Light-Emitting Ambipolar Organic Field-Effect Transistors. *Adv. Mater.* **2007**, *19*, 734−738.
(40) Chen, C.-T.; Marder, S. R.; Cheng, L.-T. Synthesis and Linear and Nonlinear Optical Properties of Unsymmetrical Squaraines with Extended Conjugation. *J. Am. Chem. Soc.* **1994**, *116*, 3117−3118.
(41) Santos, P. F.; Reis, L. V.; Almeida, P.; Serrano, J. P.; Oliveira, A. S.; Ferreira, L. F. V. Efficiency of Singlet Oxygen Generation of Aminosquarylium Cyanines. *J. Photochem. Photobiol., A* **2004**, *163*, 267−269.
(42) Gayathri Devi, D.; Cibin, T. R.; Ramaiah, D.; Abraham, A. Bis(3,5-diiodo-2,4,6-trihydroxyphenyl)squaraine: A Novel Candidate in Photodynamic Therapy for Skin Cancer Models in Vivo. *J. Photochem. Photobiol. B* **2008**, *92*, 153−159.
(43) Ramaiah, D.; Eckert, I.; Arun, K. T.; Weidenfeller, L.; Epe, B. Squaraine Dyes for Photodynamic Therapy: Mechanism of Cytotoxicity and DNA Damage Induced by Halogenated Squaraine Dyes Plus Light (>600 nm). *Photochem. Photobiol.* **2004**, *79*, 99−104.
(44) Rapozzi, V.; Beverina, L.; Salice, P.; Pagani, G. A.; Camerin, M.; Xodo, L. E. Photooxidation and Phototoxicity of π-Extended Squaraines. *J. Med. Chem.* **2010**, *53*, 2188−2196.
(45) Ahn, H.-Y.; Yao, S.; Wang, X.; Belfield, K. D. Near-Infrared-Emitting Squaraine Dyes with High 2PA Cross-Sections for Multiphoton Fluorescence Imaging. *ACS Appl. Mater. Interfaces* **2012**, *4*, 2847−2854.

(46) Sprenger, H.-E.; Ziegenbein, W. Cyclobutenediylium Dyes. *Angew. Chem., Int. Ed.* **1968**, *7*, 530−535.
(47) Ronchi, E.; Ruffo, R.; Rizzato, S.; Albinati, A.; Beverina, L.; Pagani, G. A. Regioselective Synthesis of 1,2- vs 1,3-Squaraines. *Org. Lett.* **2011**, *13*, 3166−3169.
(48) Wu, J.; Huo, E.; Wu, Z.; Lu, Z.; Xie, M.; Jiang, Q. Novel Poly(fluorene-alt-squaraine) Derivatives Having Large Coverage with Solar Spectrum. *e-Polym.* **2007**, *77*, 1−10.
(49) Kuster, S.; Geiger, T. Strategies and Investigations on Bridging Squaraine Dye Units. *Dyes Pigm.* **2012**, *95*, 657−670.
(50) Yagi, S.; Nakasaku, Y.; Maeda, T.; Nakazumi, H.; Sakurai, Y. Synthesis and Near-Infrared Absorption Properties of Linearly π-Extended Squarylium Oligimers. *Dyes Pigm.* **2011**, *90*, 211−218.
(51) Funabiki, K.; Mase, H.; Saito, Y.; Otsuka, A.; Hibino, A.; Tanaka, N.; Miura, H.; Himori, Y.; Yoshida, T.; Kubota, Y.; et al. Design of NIR-Absorbing Simple Asymmetric Squaraine Dyes Carrying Indoline Moieties for Use in Dye-Sensitized Solar Cells with Pt-Free Electrodes. *Org. Lett.* **2012**, *14*, 1246−1249.
(52) Wang, Z.; Zhang, W.; Tao, F.; Kai, G. M.; Long, Y. X.; Ying, L.; Qing, J. Synthesis and Properties of Two Novel Copolymers Based on Squaraine and Fluorene Units for Solar Cell Materials. *Chin. Chem. Lett.* **2011**, *22*, 1001−1004.
(53) Lin, V. S.-Y.; DiMagno, S. G.; Therien, M. J. Highly Conjugated, Acetylenic Bridged Porphyrins: New Models for Light-Harvesting Antenna Systems. *Science* **1994**, *264*, 1105−1111.
(54) Lin, V. S.-Y.; Therien, M. J. The Role of Porphyrin-to-Porphyrin Linkage Topology in the Extensive Modulations of the Absorptive and Emissive Properties of a Series of Ethynyl- and Butadiynyl-Bridged Bis- and Tris(porphinato)zinc Chromophores. *Chem.—Eur. J.* **1995**, *1*, 645−651.
(55) Webster, S.; Odom, S. A.; Padilha, L. A.; Przhonska, O. V.; Peceli, D.; Hu, H.; Nootz, G.; Kachkovski, A. D.; Matichak, J.; Barlow, S.; et al. Linear and Nonlinear Spectroscopy of a Porphyrin-Squaraine-Porphyrin Conjugated System. *J. Phys. Chem. B* **2009**, *113*, 14854−14867.
(56) Fixler, D.; Namer, Y.; Yishay, Y.; Deutsch, M. Influence of Fluorescence Anisotropy on Fluorescence Intensity and Lifetime Measurement: Theory, Simulations and Experiments. *IEEE Trans. Biomed. Eng.* **2006**, *53*, 1141−1152.
(57) Birks, J. B.; Dyson, D. The Relations Between the Fluorescence and Absorption Properties of Organic Molecules. *Proc. R. Soc. London, Ser. A* **1963**, *275*, 135−148.
(58) Sheik-Bahae, M.; Said, A. A.; Wei, T. H.; Hagan, D. J.; Van Stryland, E. W. Sensitive Measurement of Optical Nonlinearities Using a Single Beam. *IEEE J. Quantum Electron.* **1990**, *26*, 760−769.
(59) Reddington, M. V. Synthesis and Properties of Phosphonic Acid Containing Cyanine and Squaraine Dyes for Use as Fluorescent Labels. *Bioconjugate Chem.* **2007**, *18*, 2176−2190.
(60) Magde, D.; Brannon, J. H.; Cremers, T. L.; Olmsted, J. Absolute Luminescence Yield of Cresyl Violet. A Standard for the Red. *J. Phys. Chem.* **1979**, *83*, 696−699.
(61) Lakowicz, J. R. Resolution of Electronic States from Polarization Spectra. In *Principles of Fluorescence Spectroscopy*, 3rd ed.; Kluwer Academic/Plenum Publishers: New York, 2006; pp360−361.
(62) Yan, L.; Chen, X.; He, Q.; Wang, Y.; Wang, X.; Guo, Q.; Bai, F.; Xia, A.; Aumiler, D.; Vdovic, S.; et al. Localized Emitting State and Energy Transfer Properties of Quadrupolar Chromophores and (Multi)Branched Derivatives. *J. Phys. Chem. A* **2012**, *116*, 8693−8705.
(63) Lakowicz, J. R. General Solvent Effects: The Lippert-Mataga Equation. In *Principles of Fluorescence Spectroscopy*, 3rd ed.; Kluwer Academic/Plenum Publishers: New York, 2006; pp 208−210.
(64) Bayliss, N. S. The Effect of the Electrostatic Polarization of the Solvent on Electronic Absorption Spectra in Solution. *J. Chem. Phys.* **1950**, *18*, 292−296.
(65) Renge, I. Mechanisms of Solvents Shifts, Pressure Shifts, and Inhomogeneous Broadening of the Optical Spectra of Dyes in Liquids and Low-Temperature Glasses. *J. Phys. Chem. A* **2000**, *104*, 7452−7463.
(66) Tatikolov, A. S.; Costa, S. M. B. Photophysical and Aggregation Properties of a Long-Chain Squarylium Indocyanine Dye. *J. Photochem. Photobiol., A* **2001**, *140*, 147−156.
(67) Beverina, L.; Ruffo, R.; Patriarca, G.; De Angelis, F.; Roberto, D.; Righetto, S.; Ugo, R.; Pagani, G. A. Second Harmonic Generation in Nonsymmetrical Squaraines: Tuning of the Directional Charge Transfer Character in Highly Delocalized Dyes. *J. Mater. Chem.* **2009**, *19*, 8190−8197.
(68) Frisch, M. J.; Trucks, G. W.; Schlegel, H. B.; Scuseria, G. E.; Robb, M. A.; Cheeseman, J. R.; Scalmani, G.; Barone, V.; Mennucci, B.; Petersson, G. A. et al.. *Gaussian 09*, Revision C.1, Gaussian, Inc.: Wallingford CT, 2009.
(69) Mikhailov, I. A.; Bondar, M. V.; Belfield, K. D.; Masunov, A. E. Electronic Properties of a New Two-Photon Absorbing Fluorene Derivative: The Role of Hartree-Fock Exchange in the Density Functional Theory Design of Improved Nonlinear Chromophores. *J. Phys. Chem. C* **2009**, *113*, 20719−20724.
(70) Zhao, Y.; Schultz, N. E.; Truhlar, D. G. Exchange-Correlation Functional with Broad Accuracy for Metallic and Nonmetallic Compounds, Kinetics, and Noncovalent Interactions. *J. Chem. Phys.* **2005**, *123*, 161103: 1−4.
(71) Fabian, J. TDDFT-Calculations of Vis/NIR Absorbing Compounds. *Dyes Pigm.* **2010**, *84*, 36−53.
(72) Masunov, A. E. Theoretical Spectroscopy of Carbocyanine Dyes Made Accurate by Frozen Density Correction to Excitation Energies Obtained by TD-DFT. *Int. J. Quantum Chem.* **2010**, *110*, 3095−3100.
(73) Marenich, A. V.; Cramer, C. J.; Truhlar, D. G. Universal Solvation Model Based on Solute Electron Density and on a Continuum Model of the Solvent Defined by the Bulk Dielectric Constant and Atomic Surface Tensions. *J. Phys. Chem. B* **2009**, *113*, 6378−6396.
(74) Ohira, S.; Rudra, I.; Schmidt, K.; Barlow, S.; Chung, S.-J.; Zhang, Q.; Matichak, J.; Marder, S. R.; Bredas, J.-L. Electronic and Vibronic Contributions to Two-Photon Absorption in Donor-Acceptor-Donor Squaraine Chromophores. *Chem.—Eur. J.* **2008**, *14*, 11082−11091.
(75) Wiggins, P.; Williams, J. A. G.; Tozer, D. J. Excited State Surfaces in Density Functional Theory: A New Twist on an Old Problem. *J. Chem. Phys.* **2009**, *131*, 091101-1−091101-4.
(76) Cornelissen-Gude, C.; Rettig, W.; Lapouyade, R. Photophysical Properties of Squaraine Derivatives: Evidence for Charge Separation. *J. Phys. Chem. A* **1997**, *101*, 9673−9677.
(77) Gude, C.; Rettig, W. Radiative and Nonradiative Excited State Relaxation Channels in Squaraic Acid Derivatives Bearing Differently Sized Donor Substituents: A Comparison of Experiment and Theory. *J. Phys. Chem. A* **2000**, *104*, 8050−8057.
(78) De Miguel, G.; Marchena, M.; Zitnan, M.; Pandey, S. S.; Hayase, S.; Douhal, A. Femto to Millisecond Observations of Indole-Based Squaraine Molecules Photodynamics in Solution. *Phys. Chem. Chem. Phys.* **2012**, *14*, 1796−1805.
(79) Brooks, B. R.; Schaefer, H. F., III. Sudden Polarization: Pyramidalization of Twisted Ethylene. *J. Am. Chem. Soc.* **1979**, *101*, 307−311.